JOURNAL OF MATERIALS SCIENCE 26 (1991) 3603–3612

Energetic and kinetic evaluations conducted in Cu–3.34 at % Sn through differential scanning calorimetry

A. VARSCHAVSKY
Universidad de Chile, Facultad de Ciencias Físicas y Matemáticas, Instituto de Investigaciones y Ensayes de Materiales (IDIEM), Casilla 1420, Santiago, Chile

Microcalorimetric enthalpy measurements associated with the different peaks appearing during linear heating of Cu–3.34 at % Sn were made in a 50% cold-rolled alloy. Unlike the situation in the deformed material, quenched and furnace-cooled alloys do not exhibit thermal events at any of the heating rates employed in the temperature range scanned. In the cold-rolled condition, from the energetic and kinetic analysis of the first exothermic peak, designated Stage 1, and of the endothermic peak, designated Stage 3, it was consistently inferred that they correspond, respectively, to the growth on dislocations of a metastable phase ε' and to its subsequent dissolution prior to recrystallization. Such inference was also supported by Vickers microhardness and yield-stress determinations. The calculated volume fraction for ε' after Stage 2 goes to completion, is about 0.02. A suitable expression previously developed for enthalpy release due to the pinning of solute atoms to partial dislocations was applied to compute dislocation density from the exothermic peak (Stage 2). The calculated value is in excellent agreement with those obtained from the analysis of the recrystallization trace (Stage 4) and from tensile tests, thus confirming that the second DSC trace actually corresponds to the solute segregation process. It is also suggeseted that additional dislocation-induced formation of ε' might take place as a consequence of the enhanced solute concentration around partial dislocations. The non-isothermal dissolution kinetics of ε' was adequately described by an integrated kinetic model function essentially appropriate for application in one-dimensional diffusion situations.

1. Introduction

Cu–3.34 at % Sn (6 wt %) is a commercial alloy used for bronze casting in mechanical industries owing to its high strength, wear-corrosion- and fatigue-resistance [1]. Most of the studies on this alloy concerning the solute influence on mechanical properties, examine dynamic strain ageing phenomena [2–4]. However, growth conditions of equilibrium phase ε (or a possible metastable phase ε') predicted by the phase diagram [5] are not well documented. It is also expected that the large value of the atomic size misfit exhibited by Cu–Sn alloys [6] should produce important solute pinning effects on partial dislocations, chiefly under deformed conditions [7, 8].

Because the above features may take place over a wide range of temperatures and, also, be subjected to overlapping effects, differential scanning calorimetry (DSC) is an appropriate technique for evaluating each of these processes. In fact it has been shown that this technique is appropriate for research on annealing and ageing phenomena [9–14], dislocation density determinations and solute segregation to dislocations [15, 16] and grain boundaries [17], not only because of its simple and straightforward application, but mainly because the measured quantity (enthalpy) is directly connected with the process under investigation, in comparison with other methods which in general can give only a rather indirect indication for most solid-state processes. Enthalpy evolution or absorption takes place in such processes and can be detected before the changes in structure (ordered domains, precipitates, etc.) relating to it, become observable by other means. The way in which this enthalpy is released or absorbed has also been proved to be quite sensitive to non-localized variations in particle type, size, and volume fraction [18, 19]. In addition, information concerning reaction kinetics is supplied by the thermograms. Several reviews are available [20–22].

2. Materials and experimental procedure

The alloy employed in this study was prepared in a Baltzer VSG 10 vacuum induction furnace from electrolytic copper (99.95% purity) and tin (99.9% purity). Chemical analysis showed that this alloy contained 3.34 at % Sn. The ingot was subsequently hot-forged at 1123 K to a thickness of 20 mm, pickled with a nitric acid solution (15%) in distilled water to remove

0022–2461/91 $03.00 + .12

surface oxide, annealed at 1123 K for 72 h to achieve homogeneity, and cooled in the furnace to room temperature. Then the ingot was cold-rolled to 2.0 mm thickness with intermediate anneals at 1123 K for 1 h. After the last anneal the material was finally cold-rolled to 1.0 mm thickness (50% reduction).

For material batches to be used in the non-deformed condition, a subsequent heat treatment was performed at 923 K for 1 h. Other batches were simply furnace-cooled at a rate of 10 K h^{-1}.

Microcalorimetric analysis of the samples was performed in a Dupont 2000 thermal analyser. Specimen discs, 1.0 mm thick and 6 mm diameter, were prepared for each material condition. DSC measurements of the heat flow were made by operating the calorimeter in the constant-heating mode (heating rates of 0.833, 0.333, 0.166 and 0.083 K s^{-1}). Tests were carried out from room temperature to 860 K. To increase the sensitivity of the measurements a high-purity, well-annealed copper disc whose mass was approximately equal to that of the sample, in which no thermal events occur over the range of temperatures scanned, was used as a reference in each case. In order to minimize oxidation, dried nitrogen was passed through the calorimeter (0.8×10^{-4} m^3 min^{-1}). After each test the data were converted to a differential-heat-capacity-versus-temperature form using a previously established calibration for the DSC cell. Subsequently a linear baseline was subtracted from the data. This baseline represents the temperature-dependent heat capacity of the Cu–Sn solid solution in the existing thermal conditions, and its value was in agreement with the Kopp–Neumann rule.

Heat capacity remainder, namely differential heat capacity, ΔC_p, represents the heat associated with the solid-state reactions that take place during the DSC run. Thus the reaction peaks in the ΔC_p versus T curves can be characterized by a reaction enthalpy of a particular event.

Tensile tests were performed at room temperature on standard specimens 1.5 mm thick, 6.4 mm wide and 135 mm long (gauge length) after each of the isothermal anneals indicated in Section 3.2. The specimens were spark-cut machined from alloy sheets previously 50% cold-rolled. The mechanical property data were determined using an Instron machine at a crosshead speed of 0.4 mm min^{-1}, and the yield-stress was taken at the 0.2% offset.

3. Results

3.1. DSC thermograms

Typical thermograms at the indicated heating rates are shown in Fig. 1 by the differential heat capacity, ΔC_p, versus temperature curves for the deformed material condition. They are characterized by three exothermic reactions, Stages 1, 2, 4, and an endothermic reaction, designated Stage 3. Unlike the quenched and furnace-cooled alloys, no thermal events take place in the temperature range scanned, as shown in the thermograms of Fig. 2.

The peak occurring at higher temperatures, namely Stage 4, has been reported in the literature for deformed materials in connection with recrystallization by analogy with other alloy systems [15, 16, 23]. The thermal events associated with the other stages (1, 2 and 3) concern non-identified processes on which the present study is mainly focused.

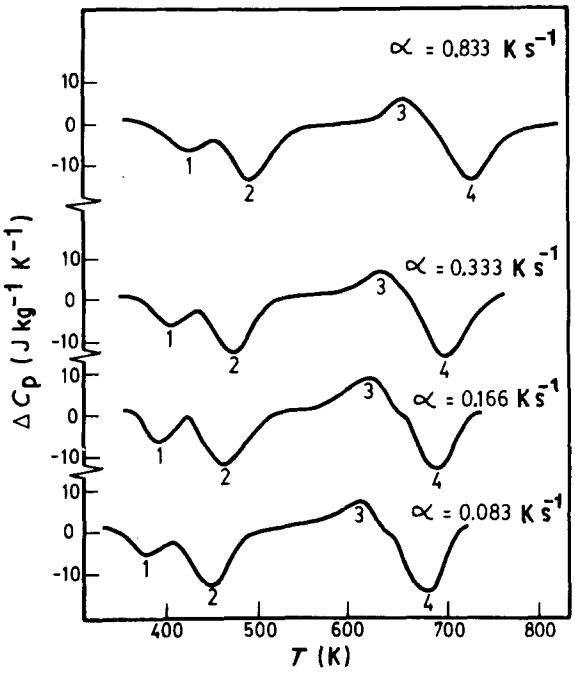

Figure 1 DSC thermograms for Cu–3.34 at % Sn, 50% cold-rolled at the indicated heating rates.

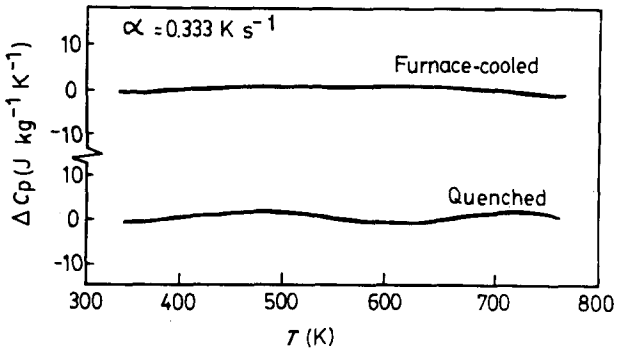

Figure 2 DSC thermograms for non-deformed Cu–3.34 at % Sn alloys.

Because Stages 1 and 2 overlap to some extent, both were separated as follows. Some samples were isothermally annealed for 1 h at the peak temperatures of Stage 1 corresponding to each of the heating rates employed. Therefore the thermal event associated with this stage took place under isothermal conditions in these specimens. When such specimens were subsequently introduced in the calorimeter and heated under non-isothermal conditions, thermograms like that displayed in Fig. 3b for instance were obtained. This figure shows the total lack of Stage 1. By subtracting the thermogram of Fig. 3b from that of Fig. 3a (which is as in Fig. 1 with $\alpha = 0.333$ K s^{-1}), Stage 1 becomes isolated as shown in the DSC trace of Fig. 3c for this heating rate. This procedure, repeated for all other heating rates, assumes that Stages 1 and 2 do not interact mutually at the annealing temperature.

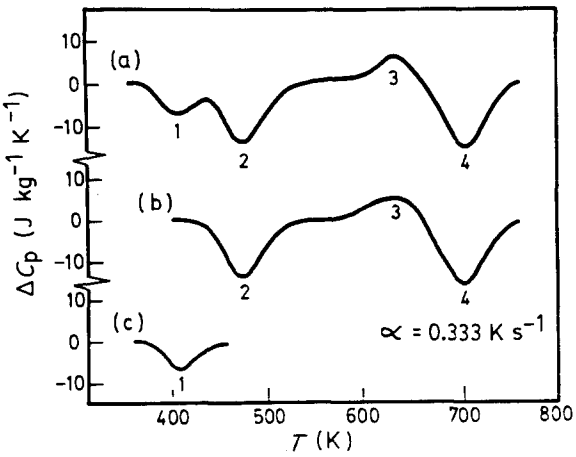

Figure 3 DSC thermograms for Cu–3.34 at % Sn (a) 50% cold-rolled, (b) as (a) but previously annealed at 383 K for 1 h. (c) Thermogram resulting from the difference of those in (a) and (b).

The areas under the ΔC_p versus T curves corresponding to the enthalpies, ΔH, of the different reactions, are listed in Table I. Subscripts indicate the stages involved. It can be noticed that $|\Delta H_1|$ is similar to $|\Delta H_3|$, thus suggesting that Stages 1 and 3 are closely related and that dislocations play a decisive role in all the stages developed because, as seen above, DSC traces are flat in the quenched as well as in the furnace-cooled materials.

Inspection of the DSC thermograms together with the enthalpimetric measurements indicate at a first glance that the exothermic peak corresponding to Stage 1 can be attributed to the formation of a metastable phase that will be designated ε′ and that nucleates and grows on dislocations (probably as Cu_3Sn, the composition of ε phase [24]). This inference can be sustained solely on a non-isothermal calorimetric basis owing to the presence of the complementary endothermic peak (Stage 3) characterized by an enthalpy absorption similar to that evolved during Stage 1. The existence of such complementary traces is typical of a growth–dissolution process taking place during a rising-temperature DSC scan [15, 16]. On the other hand, extrapolating the initial temperature of Stage 3 to $\alpha = 0$ in Fig. 4 gives an approximate value of 543 K, which is almost 20 K below the temperature given by ε solvus measured on the phase diagram [5]. This finding provides additional support to the ideas that Stage 3 corresponds to the dissolution of ε′ and, also, that this phase is metastable because otherwise both solvus temperatures would be equal.

The following sections will further analyse Stages 1 and 3 and mainly Stage 2, chiefly through kinetic and energetic evaluations. Stage 4 will provide valuable data for such analysis.

3.2. Complementary microhardness and yield-stress determinations

Vickers microhardness measurements were performed on six DSC samples for the deformed material using a load of 50 gf for 20 s. Five of these samples were successively introduced into the calorimeter at a heating rate of 0.333 K s^{-1}. The microhardness of the sixth sample was measured in the initial cold-rolled condition. Each heated specimen was extracted at the final temperature of the different peaks and the corresponding microhardness value was obtained at room temperature. Fig. 5 shows the temperatures at which the samples were removed from the differential scanning calorimeter, and the fact that the nature attributed to Stage 1 (nucleation and growth of ε′ at dislocations) is consistent with the measured hardness increase from 268.4–274.5 HV. After the additional increase in hardness observed when Stage 2 is completed, softening takes place at the beginning of Stage 3 from 286.4 to 279 HV, which can be ascribed, in principle, to a certain amount of recovery. Further softening from 279–272 HV occurs during Stage 3, consistent with the attributed dissolution of ε′. Unequivocally, Stage 4 is connected with recrystallization, as microhardness decreases from 272–133.6 HV.

TABLE I Enthalpies associated with the stages observed in deformed Cu–3.34 at % Sn

Heating rate (K s^{-1})	$-\Delta H_1$ (J mol^{-1})	$-\Delta H_2$ (J mol^{-1})	ΔH_3 (J mol^{-1})	$-\Delta H_4$ (J mol^{-1})
0.833	17.0	44.3	17.9	50.3
0.333	16.6	44.7	19.3	45.6
0.166	17.7	47.4	18.9	39.9
0.083	16.7	49.0	19.9	48.6

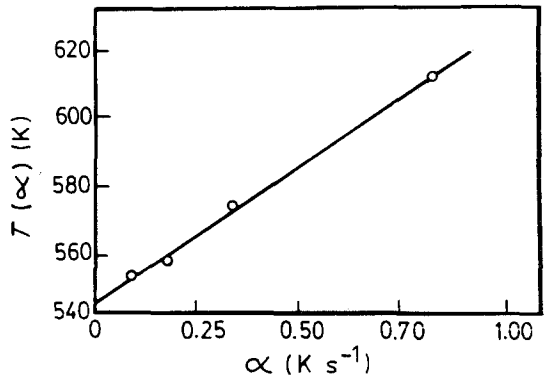

Figure 4 Initial temperature of Stage 3 as a function of heating rate.

Tensile tests at room temperature were carried out on specimens annealed for 1 h at the temperature at which each stage goes to completion. Stress–strain curves are shown in Fig. 6, where numbers refer to the stages considered. Curve D corresponds to the material in the initial cold-rolled condition. A good correlation exists between Vickers microhardness and yield-stress determined from such a curve at 0.2% offset. Both measurements indicate that Stage 2 is associated with a strengthening effect larger than that produced by Stage 1, wherein the pre-existing dislocations play a crucial role.

Furthermore, it is important to notice that hardness increase, $\Delta(HV)_1 = 6.1$ during Stage 1 is very close to its decrease $\Delta(HV)_3 = -7$ during the complementary Stage 3. These findings together with the enthalpimetric measurements provide stronger evidence that

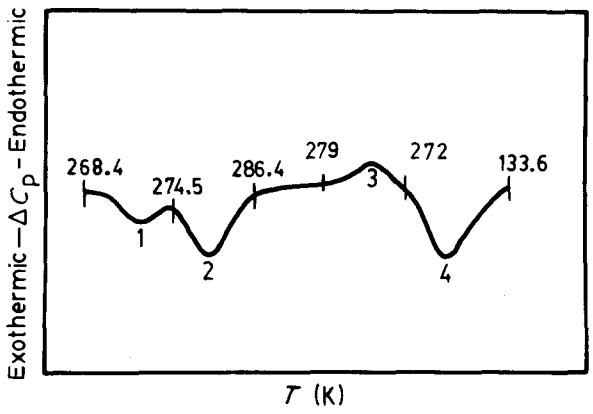

Figure 5 DSC thermograms for Cu–3.34 at % Sn, 50% cold-rolled, showing room-temperature Vickers microhardness values after heating the samples to the point indicated on the trace ($\alpha = 0.333\ K\,s^{-1}$). The scatter of measured values, as the temperature increases along the DSC scan quoted at 95.5% confidence limits are ±5.1, ±5.4, ±5.0, ±5.3, ±5.2 and ±2.8, respectively.

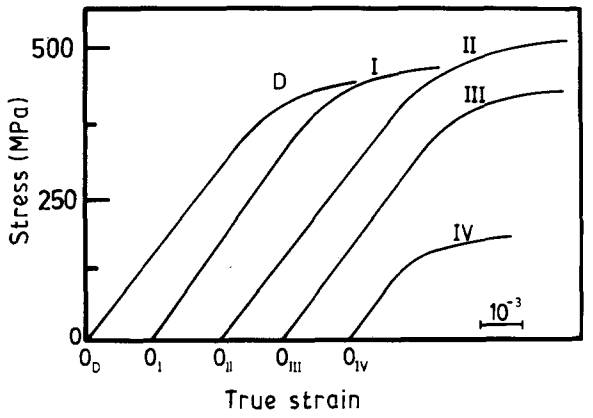

Figure 6 Plots of tensile tests on samples annealed for 1 h at the final temperature of each Stage. Curve D corresponds to the material in the initial cold-rolled condition.

Stages 1 and 3 correspond to phase transitions associated with the growth and dissolution of ε′.

In order to provide a first insight into the nature of Stage 2, a deeper description of Stages 1 and 3, as well as useful quantitative information deriving therefrom, a kinetic analysis of these stages will be performed in the following section.

3.3. Kinetic analysis

This kinetic analysis of Stage 1 is based on the concepts that underlie the theoretical model of a phase transformation involving nucleation and growth [25, 26].

In the present instance the fraction of the product phase formed at a certain time, t, is given by the well-known equation of Mehl–Johnson–Avrami obtained under isothermal conditions [25]

$$y = 1 - \exp\left\{-\left[k_0 \exp\left(-\frac{E}{RT}\right)t\right]^n\right\} \quad (1)$$

where E is the activation enthalpy of the process, T is absolute temperature, R is the gas constant, and k_0 is a pre-exponential factor.

Stage 2 has been analysed using the same model for comparison purposes. This choice can be justified because it has been shown that Equation 1 is applicable to other reactions ([26], p. 542) provided n ranges between specific values depending on the corresponding event.

Activation enthalpies are determined by the Kissinger method [27] valid for the selected kinetic model [28]. Hence such enthalpies can be computed from plots of $\ln(\alpha/T_p^2)$ versus $1/T_p$ where α is the heating rate and T is the temperature of the maximum transformation rate. These plots give straight lines of slope $-E/R$ shown in Fig. 7.

In order to determine the constants n and k_0, the usual approach to non-isothermal kinetics [21] was followed. Under such conditions the reacted fraction from Equation 1 becomes

$$y = 1 - [\exp - (k_0\theta)^n] \quad (2)$$

where θ is the reduced time [29] that can be interpreted as the time at which the reaction goes to completion at an infinite temperature. Its value can be calculated from the knowledge of E and of a $p(x)$ function [30] at a certain temperature and heating rate because

$$\theta = \frac{E}{\alpha R}\,p(x) \quad (3)$$

where $x = E/RT$ and

$$p(x) = (x + 2)^{-1}\,x^{-1}\exp(-x) \quad (4)$$

if the three-term Schlomilch expression [29] is used. Taking natural logarithms in Equation 2 and rearranging gives

$$\ln\{\ln[1/(1 - y)]\} = n\ln\theta + n\ln k_0 \quad (5)$$

Therefore, a plot of $\ln\{\ln[1/(1-y)]\}$ versus $\ln\theta$ should give a straight line of slope n and an intercept equal to $n\ln k_0$ if the kinetic law applied is correct. It can be shown that n and k_0 are essentially independent of α for the different heating rates used. Such plots are shown in Fig. 8 for $\alpha = 0.333\ K\,s^{-1}$ using the data from each corresponding thermogram in Fig. 3 and E values previously computed for both stages. Kinetic parameters E, n and k_0 are listed in Table II.

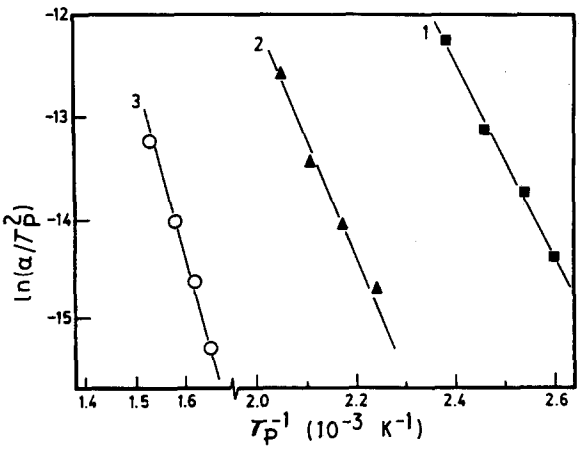

Figure 7 Kissinger plots for evaluating the activation energy of Stages 1, 2 and 3.

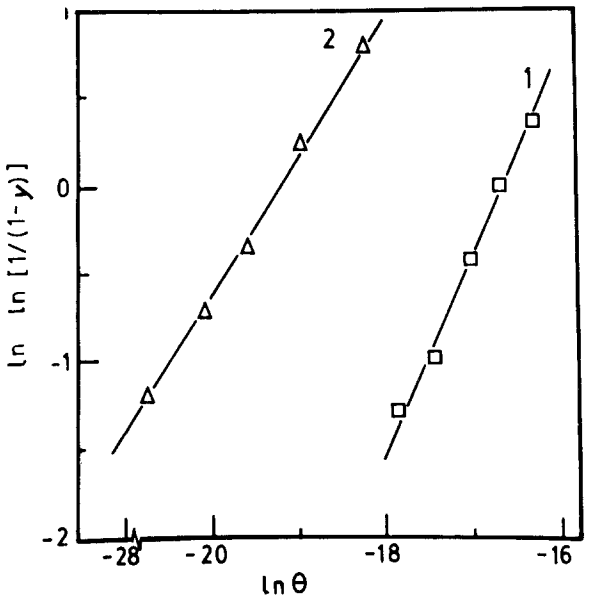

Figure 8 Plots of $\ln\{\ln[1/1(1-y)]\}$ against $\ln\theta$ for Stages 1 and 2.

TABLE II Kinetic parameters for Stages 1 and 2

Stage	E(kJ mol^{-1})	n	k_0(s^{-1})
1	87.7	1.10	1.69×10^7
2	107.0	0.72	2.20×10^8
3	168.7	–	–

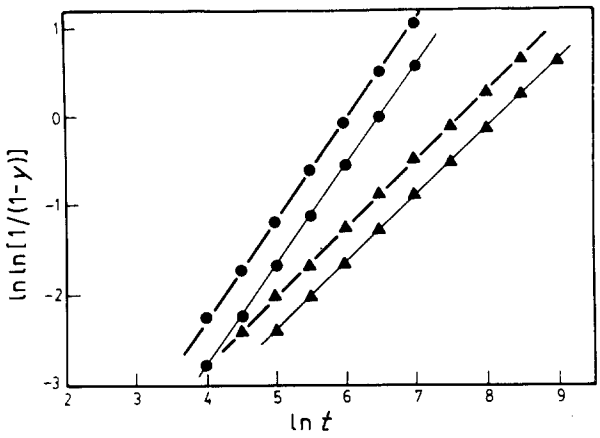

Figure 9 Plots of $\ln\{\ln[1/1(1-y)]\}$ against $\ln t$ for Stages (●) 1 and ▲ 2 at (——) 405 K and (– – –) 413 K.

The transferability principle is applied below, i.e. kinetic parameters obtained from anisothermal experiments are also valid for describing isothermal situations. Thus, in order to estimate temperature influence on the kinetics of Stages 1 and 2 the corresponding values of E, n and k_0 were introduced in the Mehl–Johnson–Avrami equation and plots of $\ln\{[\ln 1/(1-y)]\}$ versus $\ln t$ for 405 and 413 K were drawn as shown in Fig. 9. This isothermal representation shows that the reaction associated with Stage 2 at a given temperature proceeds slower than the growth of ε′ on dislocations.

Activation enthalpy for Stage 3 was also computed from a Kissinger plot and the corresponding value is included in Table II. The kinetic analysis of this stage

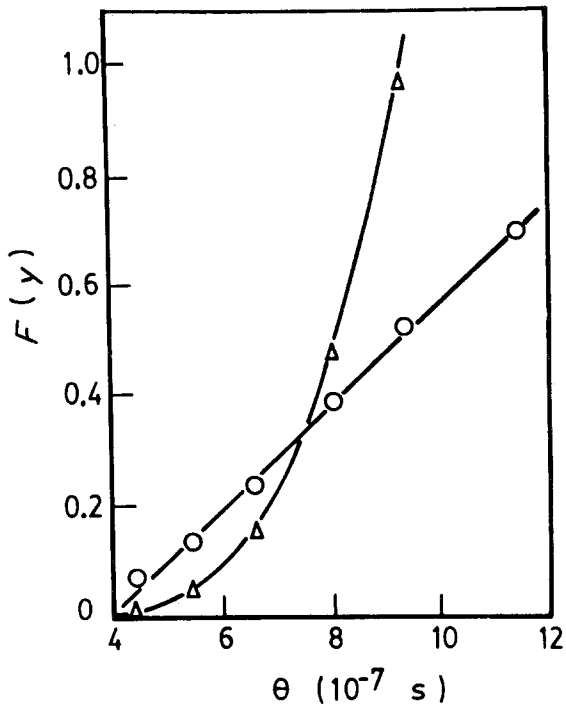

Figure 10 Plots of two integrated kinetic functions against θ. (○) $F(y)=[1-(1-y)^{1/3}]^2$, (△) $F(y)=1-(1-y)^{2/3}$.

was performed on the basis of a non-isothermal precipitate dissolution kinetic approach already discussed in earlier papers [31, 32]. In such an approach, three-dimensional diffusion-controlled situations are essentially described by means of the expression $1-(1-y)^{2/3}=k_1\theta$ while one-dimensional diffusion situations are better described by means of $[1-(1-y)^{1/3}]^2=k_2\theta$ where k_1 and k_2 are constants. The results of plotting against θ the left-hand side terms of both expressions, called integrated kinetic functions $F(y)$, are shown in Fig. 10. It is clearly seen in this figure that the dissolution behaviour of ε′ is adjusted to the model suitable for a planar interface and a one-dimensional diffusion situation, which is consistent with thin disc-like precipitates.

3.4. Segregation of tin atoms to dislocations

The kinetic analysis of Stage 2 gave $n = 0.72$, which is sufficiently small to be compatible with a process involving nucleation and growth ([26], p. 542). Besides, the resulting activation enthalpy amounting to 107.0 kJ mol^{-1} was much lower than that required for interdiffusion, E_{sd}, i.e. about 173.5 kJ mol^{-1} from the Brown and Ashby correlations [33].

In contrast, according to certain theoretical considerations ([26], p. 542) an n value of 0.66 is expected if the process involved is attributable to the segregation of solute atoms to dislocations. However, this argument alone is insufficient to ensure that the energy evolved during Stage 2 is inherent to such a process. Hence, some computations based on an enthalpy model will be performed with the aim of exploring this point in more detail. First, the enthalpy associated with the segregation of solute atoms to partial dislocations will be evaluated. Actually it represents an

Helmholtz free energy, but usually is considered to be an energy to a fair approximation [34]. Then it will be ascertained whether this process can account for reasonable computed values of dislocation densities expected for the deformation degree of the alloy.

As is well-known in these alloys, unit dislocations split even at very low tin concentrations [35]. Thus, for a dissociated dislocation in pure copper $w_s/\boldsymbol{b} = 5$ [36], w_s being the fault width and $\boldsymbol{b}$ the Burger's vector. Such a w_s value is sufficiently large to allow considering the pinning of each partial dislocation rather than that of the pair. Owing to the crystallography of fcc structure one or both partial dislocations will have a first-order misfit with a substitutional solute atom. Thus through misfit interaction, a tin atom may interact with both dissociated edge dislocations and dissociated screw dislocations.

Consider now a dislocation with its line along the vector $\boldsymbol{l}$; edge component of $\boldsymbol{b}$ is $\boldsymbol{b}_e$ normal to $\boldsymbol{l}$ and screw component is $\boldsymbol{b}_s$ and $\boldsymbol{l}$, a solute atom located at r, θ interacts with the dislocation with interaction enthalpies, ΔH_a, due to the misfit, and ΔH_m due to the modulus interaction. Expressions for ΔH values have been given by Eshelby [37] and Saxl [38]; in order to evaluate these ΔH values, the terms

$$e_a = \frac{\mathrm{d}(\ln a)}{\mathrm{d}\bar{c}} \tag{6}$$

$$e_G = \frac{\mathrm{d}(\ln G)}{\mathrm{d}\bar{c}} \tag{7}$$

$$e_k = \frac{\mathrm{d}(\ln k)}{\mathrm{d}\bar{c}} \tag{8}$$

as $\bar{c} \to 0$, which define the changes in lattice parameter a_0, in shear modulus G and in bulk modulus k, produced by a solute atom fraction $\bar{c}$, must be known.

The diverse contributions to interaction enthalpy, in terms of Poisson's ratio, ν, are as follows. For the misfit interaction with an edge component b_e they are

$$\Delta H_a = \frac{2^{1/2}(1+\nu)}{2(1-\nu)} Gb^3 \frac{b_e}{r} e_a \sin\theta \tag{9}$$

$$\Delta H_G = \frac{2^{1/2}}{16\pi^2} Gb^3 \frac{b_s}{r} e_G \tag{10}$$

and

$$\Delta H_k = 0 \tag{11}$$

For the modulus interaction with the screw component b_s they are

$$\Delta H_a = 0 \tag{12}$$

$$\Delta H_G = \frac{2^{1/2}}{16\pi^2}\left(\frac{1}{1-\nu}\right)^2 Gb^3\left(\frac{b_e}{r}\right)^2 \times e_G[1 - \tfrac{2}{3}\sin^2\theta(1 + 2\nu - 2\nu^2)] \tag{13}$$

$$\Delta H_k = \frac{2^{1/2}}{16\pi^2}\left(\frac{1-2\nu}{1+\nu}\right)^2 kb^3 \frac{b_e}{r} e_k \sin^2\theta \tag{14}$$

and thus the total modulus interaction with every component of b is

$$\Delta H_m = \Delta H_G + \Delta H_k \tag{15}$$

For Cu–Sn alloys $e_a = 0.26$ was computed using the effective solute radius from King's data [39], and $e_G = 0.27$ was evaluated using Hopkin *et al.*'s value for $G(= 44.2\ \mathrm{GN\,m^{-2}})$ [40]. In order to get $e_k = 0.13$, values for k were first computed from the equation $k = (EG/3)/(3G\text{-}E)$ [40] for each alloy composition, now using Hopkin *et al.*'s E data [40]. A value of $b = 0.258$ nm was determined from lattice parameter $a_0(= 2b/2^{1/2})$ of the alloy, by weighting the values corresponding to copper and tin. For a dissociated screw dislocation with a partial edge component $3^{1/2}b/6$ and a screw component $0.5b$, the minimum value of the misfit interaction enthalpy with a tin atom at $r = b$ is $\Delta H_{as} = -12.1\ \mathrm{kJ\,mol^{-1}}$. For a dissociated edge dislocation with a partial edge component $0.5b$ and screw component $3^{1/2}b/6$ in the same alloy $\Delta H_{ae} = -20.1\ \mathrm{kJ\,mol^{-1}}$. The computed total modulus interactions are $\Delta H_m = -0.06\ \mathrm{kJ\,mol^{-1}}$ for a dissociated screw dislocation and $\Delta H_m = -0.04\ \mathrm{kJ\,mol^{-1}}$ for a dissociated edge dislocation. The value of ν was taken as 0.33 [41]. In computing ΔH_m the value of k was expressed in terms of G $(= 0.366\,k)$. Because ΔH_m is negligible when compared with ΔH_a in both instances, it follows that the corresponding maximum force between a dislocation and a solute atom is also negligible, as already confirmed [41]. Hence, ΔH_m will be omitted in the following. Above results show that ΔH_a variation depends on whether a dissociated screw or edge dislocation is considered, the pinning force being stronger for the latter. The next step is evaluating the enthalpy released during the pinning process up to the reaction ending temperature.

Assuming that edge dislocations and screw dislocations are present in equal numbers, segregation process enthalpy per mole of solute is [15]

$$\Delta H_d = \pi b^2 \rho\left[\Delta H_{ae}\exp\left(-\frac{\Delta H_{ae}}{RT_f}\right) + \Delta H_{as}\exp\left(-\frac{\Delta H_{as}}{RT_f}\right)\right] \tag{16}$$

where ρ is the dislocation density and $T_f(= 528\ \mathrm{K})$ is reaction ending temperature at which the system returns to equilibrium. Average $\Delta H_2(= \Delta H_d)$ from Table I gives a value of $-1338\ \mathrm{J\,mol^{-1}}$ of solute. The above computed data allow calculation of the dislocation density from Equation 16. Thus $\rho = 2.89 \times 10^{11}\ \mathrm{cm\,cm^{-3}}$ in good agreement with literature values [15, 42] for heavily deformed alloys. This ρ value may have been overestimated because it seems likely that some induced ε' phase is formed around dislocations assisted by solute atoms clustered around them. Thus the evolved energy associated with Stage 2 and available for the segregation process might be lower than ΔH_2.

The peculiar behaviour of this alloy in connection with the thermograms of the quenched, furnace-cooled and deformed materials is discussed in the following section.

4. Discussion

Taking into account kinetics analysis, hardness meas-

urements, yield-stress determinations, and particularly energy evaluations used to compute a reasonable value of dislocation density, it is thought that Stage 2 is compatible with the segregation process of solute atoms to partial dislocations. In order to verify the value of ρ obtained, a comparison between ΔH_4 and the energy released during recrystallization will be made. This energy can be expressed as follows [15]

$$\Delta H_R = \frac{\rho}{\rho_s}\left[\frac{Gb^2}{4\pi A}\ln\left(\frac{m}{b\rho^{1/2}}\right) + \frac{Gb^2}{10}\right] \quad (17)$$

where $m = 4$, $A = 0.85$ and $\rho_s (= 8.90 \times 10^3\ \mathrm{kg\,m^{-3}})$ is the average density of the material. The introduction of all required data in Equation 17 yields $\Delta H_R = 39.4\ \mathrm{J\,mol^{-1}}$, that is $|\Delta H_R| \simeq 0.855\ |\Delta H_4|$ using the average value of ΔH_4. This quite good agreement between both enthalpies lends further support to the idea that ΔH_2 is associated with the segregation process.

On the other hand, dislocation density can also be determined from yield stress

$$\Delta\tau = \beta G b \rho^{1/2} \quad (18)$$

where $\Delta\tau = (\sigma_3 - \sigma_4)/3$, σ_3 (before recrystallization) and σ_4 (after recrystallization) are the 0.2% offset obtained from Fig. 6, while $\beta = 0.5$ is a dimensionless parameter [43]. Equation 18 gives $\rho = 2.0 \times 10^{11}\ \mathrm{cm\,cm^{-3}}$ in excellent agreement with the value calculated using Equation 16. Thus, in view of all these findings, Stage 2 can be definitively ascribed to a segregarion process of Sn atoms to partial dislocations.

The decrease observed in microhardness between the temperatures corresponding to the end of Stage 2 and the beginning of Stage 3 (besides a certain amount of excepted recovery, as already pointed out) can be attributed to the continuous concentration decrease of segregated solute atoms [44]. Such process would occur under dynamic equilibrium conditions [45–47] when the temperature is raised during the anisothermal run. This means that, for all the heating rates employed in the present scans, diffusion is fast enough in the above-considered temperature range in which the equilibrium solute concentration is always maintained. This feature is shown by the absence of any thermal effect between Stages 2 and 3.

As already mentioned, ΔH_1 is somewhat smaller than ΔH_3 and of opposite sign. The energy $\Delta H_3 + \Delta H_1 = 2.0\ \mathrm{J\,mol^{-1}}$ might correspond to an additional degree of ε' introduced during Stage 2, presumably assisted by dislocation pipe diffusion of the solute which is segregating simultaneously. This associated amount of evolved heat produces an overestimate of only about 4% in the dislocation density computed by means of Equation 16, and this does not alter the reasons leading to the nature assigned to Stage 2.

The compatibility of Stages 1 and 3 with the growth and the dissolution of ε' has been inferred using DSC, microhardness determinations, and also the phase diagram showing that equilibrium phase ε dissolves at about 20 K higher than the dissolution temperature of ε' determined experimentally (calculated by extrapolating to $\alpha = 0$ the initial temperature of Stage 3 in Fig. 4). The fact that phase ε' grows on dislocations, together with its lower dissolution temperature, are indicative of metastability as pointed out before. The results of the kinetic analysis of ε' formation are also in agreement with the kinetic analysis of its dissolution. In fact a value $n = 1.1$ for Stage 1 is consistent with the theoretical value of $n = 1$ obtained for needles or plates exhibiting longitudinal dimensions that are small in comparison with their separation ([26], p. 542). On the other hand the integrated kinetic function describing their dissolution kinetics reveals that also particle shape corresponds to plates [31, 32]. Hence, the same shape is consistently predicted by the two appropriate kinetic laws describing their growth and dissolution. In turn these kinetic results provide further evidence for metastable phase ε' growth and subsequent dissolution during the DSC rising-temperature scans.

It is experimentally difficult to render visible, by means of microscopic methods, precipitates in alloys exhibiting high dislocation densities. Nevertheless, further ε' features such as volume fraction were indirectly estimated. In fact the solubility curve for ε [5] allows the determination, for the stable phase ε, of a dissolution enthalpy ΔH_p of $950\ \mathrm{J\,mol^{-1}}$ using the van't Hoff isochore $\ln \bar{c} = -(\Delta H_p/R)(1/T_d) + A$, where A is a constant and T_d is the dissolution temperature. As the ε' solvus is unknown, it can be assumed that ΔH_p is approximately not much larger than the corresponding value of $\Delta H'_p$ for ε'. Thus volume fraction, $V_f (= \Delta H_3/\Delta H_p)$, amounts to 0.02, which is a value somewhat underestimated, as expected from above the discussion. This low V_f value can be explained by the fact that Stage 1 takes place at temperatures low enough, so that diffusion is only assisted by the extra vacancies introduced by the deformation process. It is thus expected that the reaction leading to ε' formation, although kinetically more favourable than Stage 2 in the range of temperatures displayed, becomes incomplete. This means that the free energy, $\Delta G'_{rs}$, available for bringing the alloy to the metastable equilibrium state (the opposite to free energy increase upon ε' resolution) is decreased only by a fraction $\Delta G''_{rs}$. This fact also means that the ε' composition should be somewhat lower than that of the metastable equilibrium. These features are schematically shown in Fig. 11.

It is worth noting that the low value of V_f computed for ε' can explain the unsuccessful attempts to detect it by standard X-ray diffraction techniques.

In this study the values calculated for the activation enthalpies of Stages 1 and 2 amounted to 87.7 and $107.0\ \mathrm{kJ\,mol^{-1}}$. Although such values do not differ very much it is suggested that different mechanisms are present in both processes. In fact, as the alloy is 50% cold-rolled, point defects (probably mainly vacancies) are introduced by dislocation interactions [48]. The simple relationship between vacancy concentration, C, and strain ε_0, is $C = 10^{-4}\varepsilon_0$ [49]. As the relation between strain and deformation reduction (0.5 in this case) is $\varepsilon_0 = -\ln(1 - R)$ [49], it follows that $C = 0.7 \times 10^{-4}$. It is easily shown that this high

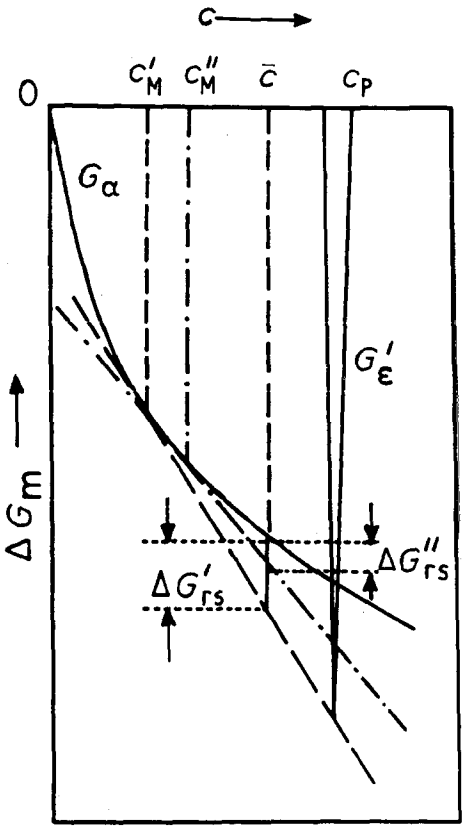

Figure 11 Schematic free-energy-composition plot for an alloy of initial concentration, $\bar{c}$, that decomposes in a matrix α containing a precipitated metastable phase ε'. $\Delta G'_{rs}$ is the free energy increase in the alloy containing $\bar{c}$ of solute ε' on resolution. c'_M is the metastable equilibrium solubility. $\Delta G''_{rs}$ is the free energy increase on ε' resolution when the reaction is incomplete, c''_M being the depleted matrix composition in this case.

vacancy concentration is equivalent to that retained in a non-deformed alloy after quenching from about 873 K. On the other hand, as it is expected that Sn atoms should attract vacancies [50] during the deformation process, very likely both free vacancies and vacancies bounded to Sn atoms will be created in excess. In principle, bounded vacancies have migration enthalpies higher than free ones by an amount at least equal to the binding enthalpy, E_{vs}, because during the multistep process of their migration a transitory disruption of the solute-vacancy-pair first neighbourhood is required if a two-dimensional square-array model is considered as a first approximation [51]. Here, before getting a deeper insight into the mechanisms through which Stages 1 and 2 are developed, E_{vs} for the alloy under study was estimated according to [52]

$$E_{vs} = \Delta H_1^\circ + (\Delta H_2^\circ - \Delta H_1^\circ) \times \left[1 - \frac{\bar{c}_2}{\bar{c}_1}\left(\frac{1 - z\bar{c}_2}{1 - z\bar{c}_1}\right)\left(\frac{\Delta H_2^\circ}{\Delta H_1^\circ}\right)\right]^{-1} \quad (19)$$

where $\Delta H_1^\circ = E_{f1} - Q_{f1}$ for solute concentration $\bar{c}_1$ and $\Delta H_2^\circ = E_{f1} - Q_{f2}$ for $\bar{c}_2$, in which E_{f1} is the formation energy of a vacancy in the pure metal, Q_f is the effective formation energy of a vacancy in the alloy, and z is the coordination number ($z = 12$). If, for instance, $\bar{c}_1 = 0.034$ and $\bar{c}_2 = 0.0574$, according to the phase diagram the temperatures of the solidus are $T_{m1} = 1168$ K and $T_{m2} = 1101$ K. For pure copper $T_m = 1357.5$ K. Taking $E_{sd}/2$ as the formation energy of a vacancy in each case, Equation 12 gives $E_{vs} = 21.2\ \text{kJ mol}^{-1}$. This value falls quite well in the range of solute vacancy binding enthalpies expected from the atomic size and valency differences between copper and tin [52].

The difference between activation energies of Stages 2 and 1 is $\Delta E = 19.3\ \text{kJ mol}^{-1}$, in reasonable agreement with the E_{vs} value computed. Hence it is suggested that the activation energy of Stage 1 corresponds to the migration energy of the excess of free vacancies and/or dislocation pipe diffusion of solute already pinned during deformation (both about $E_{sd}/2$ [53]). Instead, that of Stage 2 might correspond mainly to the migration energy of the excess of solute-bounded vacancies exhibiting short migration distances. Thus segregation takes place with a relatively low activation enthalpy ($107.0\ \text{kJ mol}^{-1}$) probably assisted by the migration of the excess of such type of complexes, and also because some interdiffusion occurs in a structure much more open than that of bulk crystal. Stacking faults might also have influence as a reservoir of solute atoms: the larger is w_s the greater the solute atom supply available for pinning.

It is worth recalling that at the relatively low temperatures at which Stage 1 is displayed the diffusion is still sufficiently slow so that the volume fractions of ε' formed are about 17% and 33% of those estimated for ε from the phase-diagram at Stages 1 and 2 completion temperatures (405 and 528 K, respectively). Owing to this it is expected that, as observed, the alloy would not decompose at all if not previously deformed, because additionally dislocations reduce energy-barrier nucleation ([53], p. 308). Stage 3 takes place with an activation energy of $168.7\ \text{kJ mol}^{-1}$ in excellent agreement with that of interdiffusion ($173.5\ \text{kJ mol}^{-1}$ [33]).

Now we will discuss why, as revealed by the amount of heat absorbed during Stage 3, the ε' volume fraction is not increased at higher temperatures. First, the free energy increase ΔG_{rs} on resolution of the equilibrium phase ε was calculated according to [54]

$$\Delta G_{rs} = RT\{\bar{c}\ln\bar{c} + (1 - \bar{c})\ln(1 - \bar{c}) - c_M \ln c_M - (1 - c_M)\ln(1 - c_M) - [\ln c_M - \ln(1 - c_M)](\bar{c} - c_M)\} \quad (20)$$

where c_M is the equilibrium solubility of the matrix at temperature T obtained from the phase diagram. Taking, for instance, $\alpha = 0.333\ \text{K s}^{-1}$, at the peak temperature of Stage 1, $\Delta G_{rs} = 215\ \text{J mol}^{-1}$, while at the final temperature of Stage 2, $\Delta G_{rs} = 48\ \text{J mol}^{-1}$ only. This means that when diffusion becomes faster the driving force for alloy decomposition is drastically reduced, thus inhibiting in principle a further increase in ε volume fraction. However, at the final temperature, $\Delta G'_{rs}$ should be actually lower because ε' is thermally less stable. In addition, after Stage 2 completion, the amount of solute available for ε' formation varies to some extent. In fact the fraction of solute atoms segregated to the partial dislocations and readily obtain-

able from

$$f_d = \pi\rho b^2\left[\exp\left(-\frac{H_{ae}}{RT_f}\right) + \exp\left(-\frac{H_{as}}{RT_f}\right)\right] \quad (21)$$

is 0.083. On the other hand, the fraction, $f_p (= c_p V_f/\bar{c})$ of solute precipitated at ε′ is about 0.15. Hence at the end of the segregation process a residual solute concentration amounting to $c_r = 0.0256$ $(= \bar{c}[1 - (f_d + f_p)])$ is available for further development of ε′. If, as pointed out before, it is assumed that the equilibrium concentration of pinned solute atoms is always maintained under dynamic equilibrium conditions between Stages 2 and 3, then c_r variation is negligible. This concentration is low enough so that together with the small free-energy barrier to ε′ dissolution, the same volume fraction reached before Stage 3 will be essentially retained.

Finally, it is necessary to elucidate why the reaction leading to ε′ phase formation occurs at temperatures lower than that of the segregation process. Such an analysis can be based on kinetic and energetic considerations. In fact, before ε′ dissolution occurs, that part of the depleted matrix composition due to the achieved volume fraction (the part due to segregation) is $c''_M = (\bar{c} - V_f c_p)/(1 - V_f)$ where $\bar{c} = 0.0334$, $V_f = 0.02$ and $c_p = 0.25$ assuming that ε′ structure is the same as that of ε, namely Cu_3Sn [24], so that these values give $c''_M = 0.029$. Then a rough estimate of binding enthalpy $\Delta E_b (= -\Delta H_3/(\bar{c} - c''_M))$ between a tin atom and an ε′ precipitate gives the value of $-43.4\,kJ\,mol^{-1}$. Here ΔE_b represents, as a first approximation, the enthalpy required to remove tin from an ε′ precipitate. However the enthalpy supplied to a segregated tin atom to remove it from a partial edge dislocation is $-20.1\,kJ\,mol^{-1}$ while it is $-13.2\,kJ\,mol^{-1}$ for a partial screw dislocation. The driving force required for ε′ precipitation is thus about twice that involved in the segregation to a partial edge dislocation. Furthermore the kinetic barrier for the former process is $19.3\,kJ\,mol^{-1}$ lower. Hence ε′ development is proceeding faster than the segregation reaction. For instance, according to the isothermal kinetic plots in Fig. 9, after 180 s at 413 K the transformed fraction is $y_d = 0.13$ for segregation, and $y_d = 0.31$ for ε′ reaction.

Acknowledgements

The author thanks his alternate investigator Eduardo Donoso for his very valuable contribution to this research work, the Fondo Nacional de Desarrollo Científico y Technológico (FONDECYT) for Contract 89-0934, and the Departamento Técnico de Investigación de la Universidad de Chile for financial support (Contract I-3110/9012). The author is also indebted to the Instituto de Investigaciones y Ensayes de Materiales (IDIEM), Facultad de Ciencias Físicas y Matemáticas, Universidad de Chile, for financial support and for the facilities provided for this research. Thanks are also due to Raymond Toledo for his help with the manuscript.

References

1. E. R. PARKER, "Materials Data Book' (McGraw-Hill, NY, 1967) p. 164.
2. B. RUSSEL and P. VELA, *Phil. Mag.* **8** (1963) 677.
3. B. RUSSEL, *ibid.* **8** (1963) 615.
4. K. W. QIAN and R. E. REED-HILL, *Acta Metall.* **3** (1983) 87.
5. "Metals Handbook", Vol. 8, 8th Edn (American Society for Metals, Metals Park, Ohio, 1973) p. 299.
6. N. BEHNOOD, R. M. DOUTHWAITE and J. T. EVANS, *Acta Metall.* **28** (1980) 1133.
7. L. DELÉHOUZÉE and A. DERUYTTERE, *ibid.* **15** (1967) 727.
8. P. C. J. GALLAGHER, *Metall. Trans.* **1** (1970) 2429.
9. E. LANG, *Z. Metallkde* **64** (1973) 56.
10. R. DE AISI and P. N. ADLER, *Metall. Trans.* **8A** (1977) 1177.
11. P. N. ADLER and R. DE AISI, *ibid.* **8A** (1977) 1185.
12. B. MAILLARD, J. J. VILLENEUVE and C. FILLIATRE, *Thermochim. Acta* **33** (1979) 107.
13. J. M. PAPAZIAN, *Metall. Trans.* **2A** (1981) 269.
14. *Idem, ibid.* **13A** (1982) 761.
15. A. VARSCHAVSKY, *ibid.* **13A** (1982) 801.
16. *Idem, Mater. Sci. Engng* **89** (1987) 119.
17. A. VARSCHAVSKY and E. DONOSO, *ibid.* **A101** (1988) 231.
18. R. J. LITVAK and J. M. PAPAZIAN, *Scripta Metall.* **18** (1984) 483.
19. E. S. BALMUTH, *ibid.* **18** (1984) 301.
20. D. DOLLIMOR, in "The State-of-the-Art of Thermal Analysis", edited by O. Menis, H. Rock and P. D. Garn, NBS Special Publication no. 580 (US Government Printing Office, Washington, DC, 1980) p. 1.
21. M. E. BROWN and C. A. R. PHILLPOTTS, *J. Chem. Educ.* **55** (1978) 556.
22. P. D. GARN, *Crit. Rev. Anal. Chem.* **3** (1972) 65.
23. J. M. POPPLEWELL and J. CRANE, *Metall. Trans.* **2** (1971) 3411.
24. W. B. PEARSON, 'Structure Reports for 1959", Published for the International Union of Crystallography, Netherlands, Vol. 23, 1965, p. 133.
25. J. BURKE, "The Kinetics of Phase Transformation in Metals", 1st Edn (Pergamon, Oxford, 1961) p. 487.
26. J. W. CHRISTIAN, "Theory of Transformation of Metals and Alloys", 2nd Edn (Pergamon, Oxford, 1975) p. 489.
27. H. E. KISSINGER, *Anal. Chem.* **28** (1957) 1702.
28. A. VARSCHAVSKY and E. DONOSO, *Metall. Trans.* **14A** (1983) 875.
29. T. OZAWA, *J. Thermal. Anal.* **9** (1976) 369.
30. C. D. DOYLE, *Nature (London)* **207** (1965) 290.
31. A. VARSCHAVSKY and E. DONOSO, *Thermochim. Acta* **69** (1983) 341.
32. *Idem, J. Mater. Sci.* **21** (1986) 3873.
33. A. M. BROWN and M. F. ASHBY, *Acta Metall.* **28** (1980) 1085.
34. J. P. HIRT and J. LOTHE, "Theory of Dislocations", 2nd Edn (Wiley, New York, 1982) pp. 512, 496, 489.
35. A. K. LAHIRI and T. BANERJEE, *Brit. J. Appl. Phys.* **16** (1965) 1217.
36. D. J. H. COCKAYNE, M. L. JENKINS and I. L. F. RAY, *Philos. Mag.* **24** (1971) 1383.
37. J. D. ESHELBY, in "Physics of Metals, Defects", Vol. 2, edited by P. B. Hirsh (Cambridge University Press, Cambridge, 1975) p. 1.
38. I. SAXL, *Czech. J. Phys. B*, **14** (1964) 381.
39. H. W. KING, *J. Mater. Sci.* **1** (1966) 79.
40. M. T. HOPKIN, H. PERSEY and M. F. MARKHAN, *Z. Metallkde* **61** (1970) 535.
41. C. T. K. KUO and R. J. ARSENAULT, *Mater. Sci. Engng* **30** (1977) 65.
42. L. M. CLAREBROUGH, M. E. HARGREAVES and M. H. LORETTO, *Proc. R. Soc. London, Ser. A* **275** (1960) 363.
43. F. HAESSNER and J. SCHMIDT, *Scripta Metall.* **22** (1988) 1917.
44. D. KUHLMANN-WILSDORF, in "Physical Metallurgy", 2nd Edn, edited by R. W. Cahn (North Holland, Amsterdam, London, 1970) p. 827.

45. A. VARSCHAVSKY and E. DONOSO, *Metall. Trans.* **15A** (1984) 1999.
46. A. VARSCHAVSKY, *J. Mater. Sci.* **20** (1985) 3881.
47. *Idem*, in "Advanced Materials Conference", edited by J. G. MORSE (The Metallurgy Society Inc., Warrendale, PA, 1987) p. 33.
48. J. L. BOCQUET, G. BRÉBEC and Y. LIMOGE, in "Physical Metallurgy", 3rd Edn, edited by R. W. Cahn and P. Hassen (North Holland, Amsterdam, Oxford, New York, Tokyo, 1983) p. 462.
49. F. SEITZ, *Adv. Phys.* **1** (1952) 43.
50. M. A. MEYERS and K. K. CHAWLA, "Mechanical Metallurgy" (Prentice-Hall, Englewood Cliffs, NJ, 1984) p. 219.
51. T. S. HUTCHISON and D. C. BAIRD, 'The Physics of Engineering Solids" (Wiley, New York, London, 1963) p. 77.
52. JIN-ICHI TAKAMURA, in "Physical metallurgy", 2nd Edn, edited by R. W. Cahn (North Holland, Amsterdam, London, 1970) p. 892.
53. P. G. SHEWMON, "Transformation in Metals", 1st Edn, (McGraw-Hill, New York, 1969) p. 65.
54. R. D. DOHERTY, *Met. Sci.* **16** (1982) 1.

Received 25 August 1989
and accepted 29 October 1990